

Article

Shale Oil Enrichment Mechanism of the Paleogene Xingouzui Formation, Jianghan Basin, China

Qiqi Li ¹, Shang Xu ^{2,*}, Liang Zhang ³, Fengling Chen ³, Shiqiang Wu ³ and Nan Bai ¹

¹ Key Laboratory of Tectonics and Petroleum Resources, Ministry of Education, China University of Geosciences, Wuhan 430074, China; liqiqi6@163.com (Q.L.); 15207162827@163.com (N.B.)

² Shandong Provincial Key Laboratory of Deep Oil & Gas, China University of Petroleum (East China), Qingdao 266580, China

³ Exploration and Development Research Institute, Sinopec Jianghan Oilfield Company, Wuhan 430074, China; zhang-l.jhyt@sinopec.com (L.Z.); chenfl.jhyt@sinopec.com (F.C.); wusq.jhyt@sinopec.com (S.W.)

* Correspondence: xushang0222@163.com

Abstract: Organic-rich lacustrine shales are widely developed in China, and they have long been simply regarded as homogeneous source rocks, which restricts the understanding of intrasource oil accumulation. At present, the study of the LXF (Lower Member of the Xingouzui Formation) in the Jianghan Basin as an unconventional oil reservoir is still in its infancy, and the hydrocarbon accumulation mechanism is still unclear. Geochemical and mineralogical studies were carried out on a suite of samples from the 100-m-thick sequence, i.e., LXF II Oil Bed, by using XRD, SEM, MICP, and Rock-Eval pyrolysis. The results show that the II Oil Bed is rich in carbonate and poor in clay, so it shows a good fracturing tendency. The high degree of heterogeneity in mineral composition leads to frequent interbedding of different lithofacies. In the II Oil Bed, intercrystalline pores, interparticle pores, and intraparticle pores are developed, and micro-fractures are often observed. However, the main pore types, pore size distribution, and connectivity are quite different among lithofacies, and the carbonate-rich lithofacies have better reservoir capacity. The OM (organic matter) abundance of the II Oil Bed varies greatly and generally ranges from fair to very good. Coupled with its early-mature to mature Type II OM, it is considered to have the characteristics required for oil generation. Comprehensive analysis shows that the II Oil Bed has good shale oil exploration prospects, and the enrichment of shale oil in the sequence is the result of multiple factors matching. Firstly, high organic matter abundance is the material basis for shale oil enrichment. Secondly, thermal maturity is a prerequisite, and the difference in burial depth leads to the differential enrichment of shale oil in different areas. Thirdly, pores and micro-fractures developed in shale not only provide space for hydrocarbon storage, but also form a flow-path network. Finally, multi-scale intrasource migrations are key processes ranging from the scale of lithofacies to the intervals, which further results in the differential shale oil enrichment in different lithofacies and intervals. Considering the hydrocarbon generation capacity and reservoir quality, the prospective depth for shale oil exploration in the study area is >1350 m. The findings of this study can help in the better-understanding of the shale oil enrichment mechanism, and the optimization of future exploration strategies.

Keywords: shale oil; enrichment mechanism; lacustrine source rocks; Jianghan Basin



Citation: Li, Q.; Xu, S.; Zhang, L.; Chen, F.; Wu, S.; Bai, N. Shale Oil Enrichment Mechanism of the Paleogene Xingouzui Formation, Jianghan Basin, China. *Energies* **2022**, *15*, 4038. <https://doi.org/10.3390/en15114038>

Academic Editor: Edo Boek

Received: 26 April 2022

Accepted: 28 May 2022

Published: 31 May 2022

Publisher's Note: MDPI stays neutral with regard to jurisdictional claims in published maps and institutional affiliations.



Copyright: © 2022 by the authors. Licensee MDPI, Basel, Switzerland. This article is an open access article distributed under the terms and conditions of the Creative Commons Attribution (CC BY) license (<https://creativecommons.org/licenses/by/4.0/>).

1. Introduction

With conventional oil and gas resources in short supply, unconventional resources with huge potential are receiving widespread attention [1–5]. Shale oil is one of the hotspots of unconventional oil and gas exploration [1]. Shale oil systems are defined as organic-rich mudstone units that produce oil that retain in situ or migrate to adjacent organic-lean rocks [1]. However, another definition strictly refers to the oil producible from organic-rich shale or mudstones. In this study, the first definition was adopted. Shale oil

resources in China are mainly distributed in the Mesozoic-Cenozoic strata of lacustrine basins [6]. It is very different from North American marine shale oil due to the complex structural conditions, unstable stratigraphic distribution, small sedimentary scale, rapid facies changes, and various reservoir types of lacustrine basins [7–11]. However, at present, the basic geological research on lacustrine shale is relatively weak and the conditions for shale oil enrichment are not clear [12]. Therefore, although some lacustrine shales may contain certain hydrocarbons, it is still unknown whether they have good shale oil exploration potential. Recent studies have shown that some lacustrine shales are also promising targets for shale oil exploration and development [13]. However, a large number of studies still focus on marine shales [1,14,15]. In contrast, relatively few studies have been conducted on lacustrine shale.

Shale oil enrichment is directly related to the properties of source rocks and reservoirs [6]. Therefore, total organic carbon (TOC) and reservoir quality are usually regarded as the main factors for shale oil accumulation, representing hydrocarbon generation potential and reservoir capacity, respectively [1]. However, further studies have found that they are closely related to mineral composition, lithology, and sedimentary structure [13]. According to the sedimentary theory, the influence of climate and tectonics on lacustrine sediments is usually multi-scale and multi-faceted [8,16]. The formation and accumulation of lacustrine shale oil also show strong heterogeneity at the multi-scale [17,18]. However, some organic-rich lacustrine sediments are still simply regarded as homogeneous source rocks, which restricts the understanding of intrasource oil accumulation.

In recent years, shale oil resources have been found in argillaceous dolomite of the Junggar Basin and the Santanghu Basin [19,20], and recently, in the argillaceous dolomite of the LXF (Lower Member of the Xingouzui Formation) in the Jiangnan Basin, which broadens the scope of shale oil exploration. However, in the exploration of the Jiangnan Basin over the past decades, the LXF has been simply regarded as the source rock of the conventional reservoirs. However, the fact is that lacustrine shales exhibit a high degree of heterogeneity on multi-scale. Due to the differences in hydrocarbon generation capacity, hydrocarbon migration, and accumulation conditions caused by the OM type, lithofacies, petrology, and petrophysics, hydrocarbons are expected to migrate from one sub-unit to another. It is still unclear whether intrasource migration is one of the processes of lacustrine shale oil enrichment, and whether it is related to the multi-scale heterogeneity of shale. In addition, the lack of basic geological research has led to a poor understanding of the factors controlling the differential shale oil enrichment in different regions. To fill this gap, this paper focuses on the investigation of the mineralogy, lithology, and organic geochemistry of the LXF. Through the comparative study of wells with different buried depths, we reveal the control effect of thermal evolution on shale oil enrichment. Taking lithofacies as the research object, the reservoir capacity, hydrocarbon generation potential of different lithofacies, and intra-source migration effect are revealed through the study of pore and geochemical characteristics. It is expected to be helpful for the optimization of future shale oil exploration strategies, and provide references for the study of shale oil under similar geological backgrounds.

2. Geological Setting

The Jiangnan Basin is a Cretaceous-Oligocene rift basin with an area of ~28,760 km², and is divided into five depressions and three uplifts [21,22] (Figure 1A). Rifting in the basin was caused by Pacific–Eurasia subduction and initiated during the Late Cretaceous period [23,24]. Since the Paleogene, the basin has experienced two rifting stages caused by the India–Eurasia collision [25].

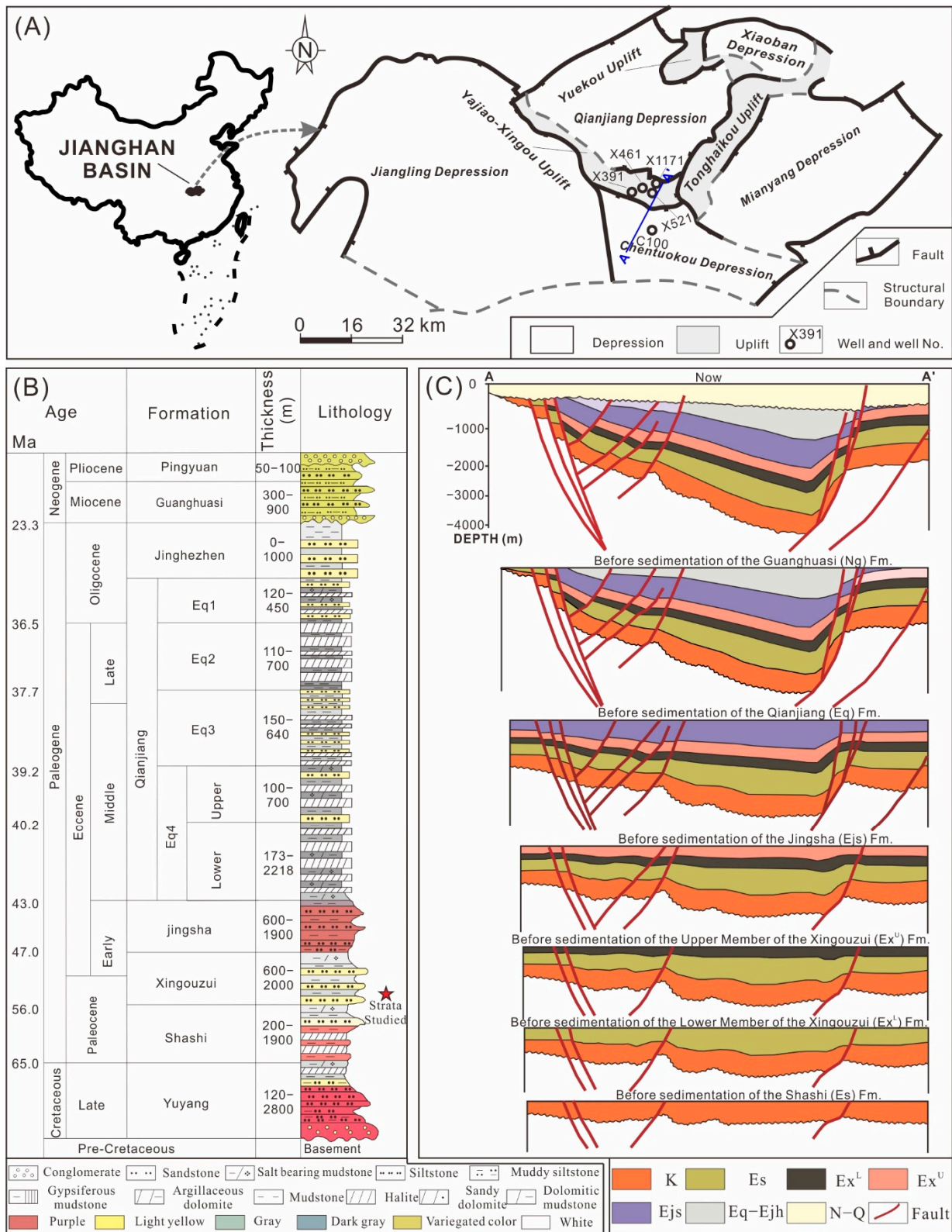


Figure 1. (A) Location and an overview map of the Jiangnan Basin. (B) Simplified stratigraphic column [21]. (C) The tectonic evolution of the study area, after the Exploration and Development Research Institute Sinopec Jiangnan Oilfield Company, 2020. Fm = Formation.

The basin is a polycyclic sedimentary basin with a basement of >7000 m, and is mainly composed of pre-Cretaceous marine and continental sedimentary rocks [21,22]. From

the Cretaceous to the Quaternary, the provenance was mainly from the northwest of the basin, and the maximum thickness of strata was >10,000 m, with obvious cyclicity and rhythmicity [22,26]. These overlying sedimentary rocks mainly include Cretaceous and Cenozoic clastic rocks and evaporites [22,27], which can be divided into seven stratigraphic units (Figure 1B). Among them, the Xingouzui Fm is one of the most important source rocks in the Jiangnan Basin [26,27].

During the deposition of the Xingouzui Fm, the sedimentary environment mainly included shallow to semi-deep water [26]. The weak tectonic activity during the deposition resulted in quite stable stratigraphic development [22]. However, post-depositional tectonic evolution has led to differences in the burial depth of the strata in different regions (Figure 1C). The LXF was deposited in a saline lacustrine environment, mainly composed of mudstone, shale, argillaceous dolomite, and dolomitic mudstone [22,26]. It was divided into four beds from bottom to top (i.e., III Oil Bed, Clay Interlayer Bed, II Oil Bed, I Oil Bed, and Gypsolyte Bed), in which the II Oil Bed with a thickness of ~100 m is the main oil-bearing strata and one of the most promising shale oil exploration targets in the Jiangnan Basin [22,27].

3. Samples and Methods

Core samples of the target layers (i.e., the II Oil Bed) were obtained from five wells (Figure 1A). Intensive sampling was performed to fully consider the heterogeneity. Bulk geochemical and mineralogical analyses were performed on all samples. Thirty-three samples were selected for MICP (mercury intrusion capillary pressure) experiments, and 42 samples for Soxhlet extraction.

The XRD (X-ray diffraction) analysis was measured with a D/max-2600/PC X-ray Diffractometer with Cu-K α radiation (40 kV, 25 mA). The quantitative analysis of the mineral composition further characterizes the basic features of the samples, and on this basis, the lithofacies of shale are divided. MICP analyses were performed using a Micromeritics 9505 Instrument at a temperature of 15 °C and a humidity of 62%, according to the standard SY/T 5346-2005. MICP analyses were used to characterize the pore characteristics of shale reservoirs, and evaluate the reservoir capacity of different lithofacies.

Rock-Eval pyrolysis was performed using a Rock-Eval 6 Instrument. The initial temperature was set at 300 °C (for 3 min), then increased to 650 °C at a rate of 25 °C/min. The main geochemical parameters obtained from the Rock-Eval analysis include TOC (total organic carbon), S1, S2, Tmax, and HI (hydrogen index), which were used to evaluate the organic matter abundance, type, and maturity of source rocks. Forty-two samples were crushed to a mesh size of 80–120, and about 120 g were taken for Soxhlet extraction for 72 h under water-bath conditions. The content of extracts (soluble organic matter) obtained was combined with Rock-Eval pyrolysis parameters to propose a new evaluation parameter to characterize the state of OM in different lithofacies.

4. Results

4.1. Mineralogy and Lithofacies

The LXF II Oil Bed predominately consists of dolomite (0–91.4%; avg. 37.01%), clay (1.3–55.7%; avg. 20.37%), and quartz (0.8–64.0%; avg. 15.75%), followed by feldspar (0–28.4%; avg. 9.66%), analcime (0–30.3%; avg. 6.06%), and anhydrite (0–89.7%; avg. 5.25%) (avg. = average). In addition, there are small amounts of pyrite (0–11.1%; avg. 1.89%) and halite (0–3.1%; avg. 0.28%) (Figure 2A). In the clay mineral component, the main species are I/S (illite/smectite mixed layer) (avg. 45.9%), illite (avg. 36.4%), and chlorite (avg. 17.2%), and trace C/S (chlorite/smectite mixed layer) (avg. 0.4%) (Figure 2B). The ternary diagram shows that, compared with typical USA shales, the LXF II Oil Bed has higher carbonate and lower clastic mineral contents, and belongs to a continental carbonate-rich shale (Figure 2C). As a result, most of the samples belong to calcareous dolomite shale (CDS) and mixed shale (MS), with only a few belonging to felsic shale (FS) or clay shale (CS) (Figure 2C).

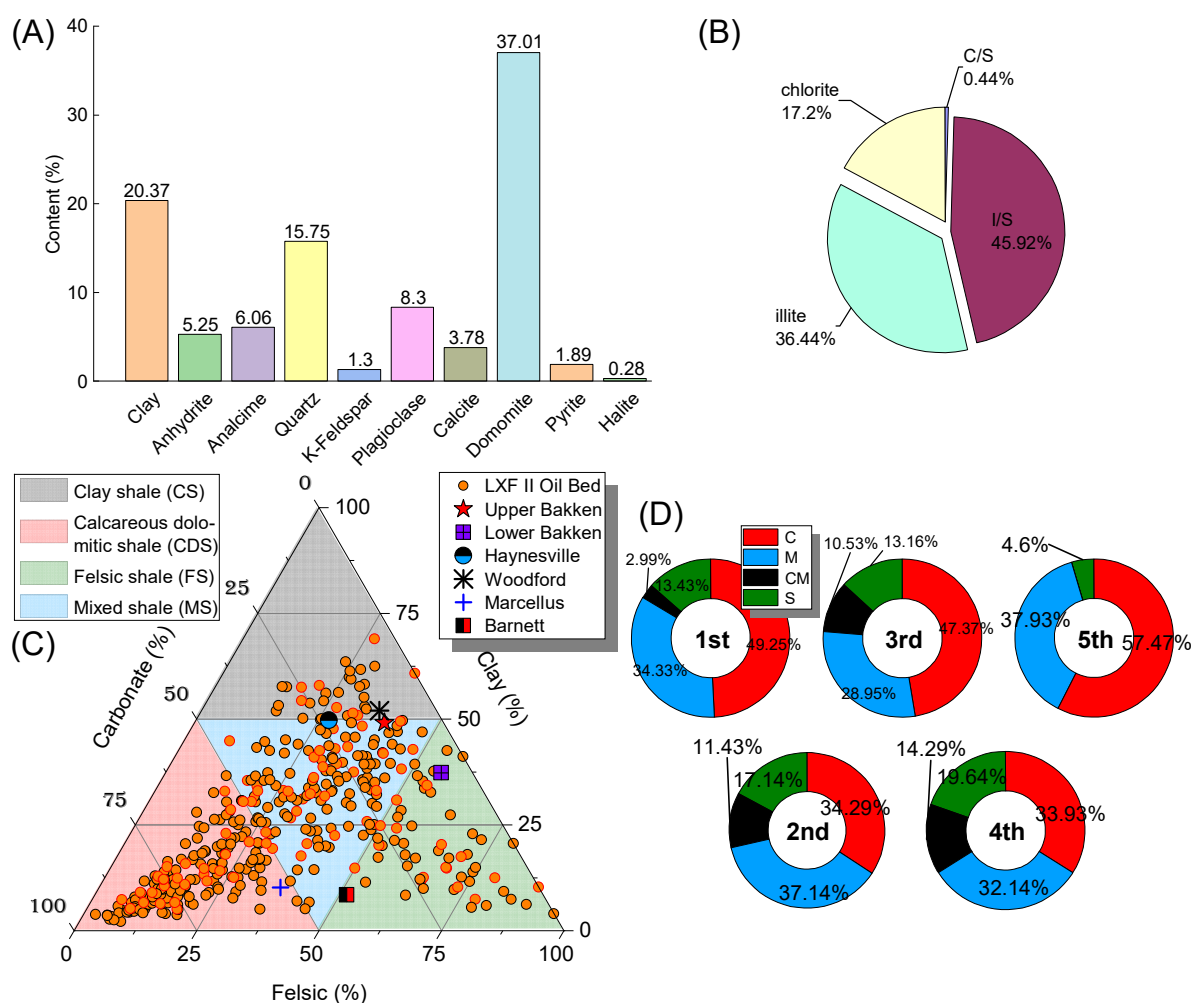


Figure 2. Mineralogical and lithofacies characteristics of the LXF II Oil Bed in the Jiangnan Basin. (A) The proportion of main minerals. (B) Types of clay minerals. (C) Ternary diagram of lithofacies division; data for comparison taken from [28,29]. (D) The proportion of various lithofacies in different intervals.

The vertical variations in mineralogy are quite significant (Figure 3). The II Oil Bed with a thickness of ~100 m has been subdivided top-down into five intervals (Figure 3), mainly based on the following reasons: a. In terms of lithology, the 1st, 3rd, and 5th intervals are characterized by frequent interbedding of argillaceous dolomite and dolomitic mudstone (Figure 4A,B); these three intervals are defined as dolomitic mixed shale sections by the Jiangnan Oilfield. In the 2nd and 4th intervals, dolomitic mudstone interbedded frequently with massive mudstone (Figure 4C), which are defined as mudstone sections by the Jiangnan Oilfield. b. On the logging curve, the 1st, 3rd, and 5th intervals have a high-frequency fluctuation, which is different from the 2nd and 4th intervals (Figure 3). c. In lithofacies, the extensive variations of mineral composition result in the vertical variation of lithofacies at the sub-meter scale. However, the 1st, 3rd, and 5th intervals are mainly composed of CDS and MS, and CDS accounts for about 50%. Although the 2nd and 4th intervals are still dominated by CDS and MS, they have more CS and FS (Figure 2D). Lamination structures are observed in MS, whereas CDS typically exhibits massive structures (Figure 4D,E). Lamination is generally interpreted as the deposition by suspension settling in relatively still and mostly stratified anoxic bottom water [30], whereas when sediments accumulate rapidly, they tend to be bedded or massive [13]. In addition, the formation of lamination requires a periodic supply of different components [31]; if the sedimentary components are relatively single, there is no obvious lamination or no lamination. Therefore,

the large supply of terrestrial debris during the flood period or the rapid precipitation of carbonate minerals during the dry period will lead to the absence of a clear lamination structure, thus showing as bedded or massive [32]. Moreover, SEM images show that solid OM are often present in MS, whereas the matrix pores of CDS are usually filled with precipitated oil (Figure 4F,G). These differences between lithofacies imply that there may be differences in shale oil enrichment.

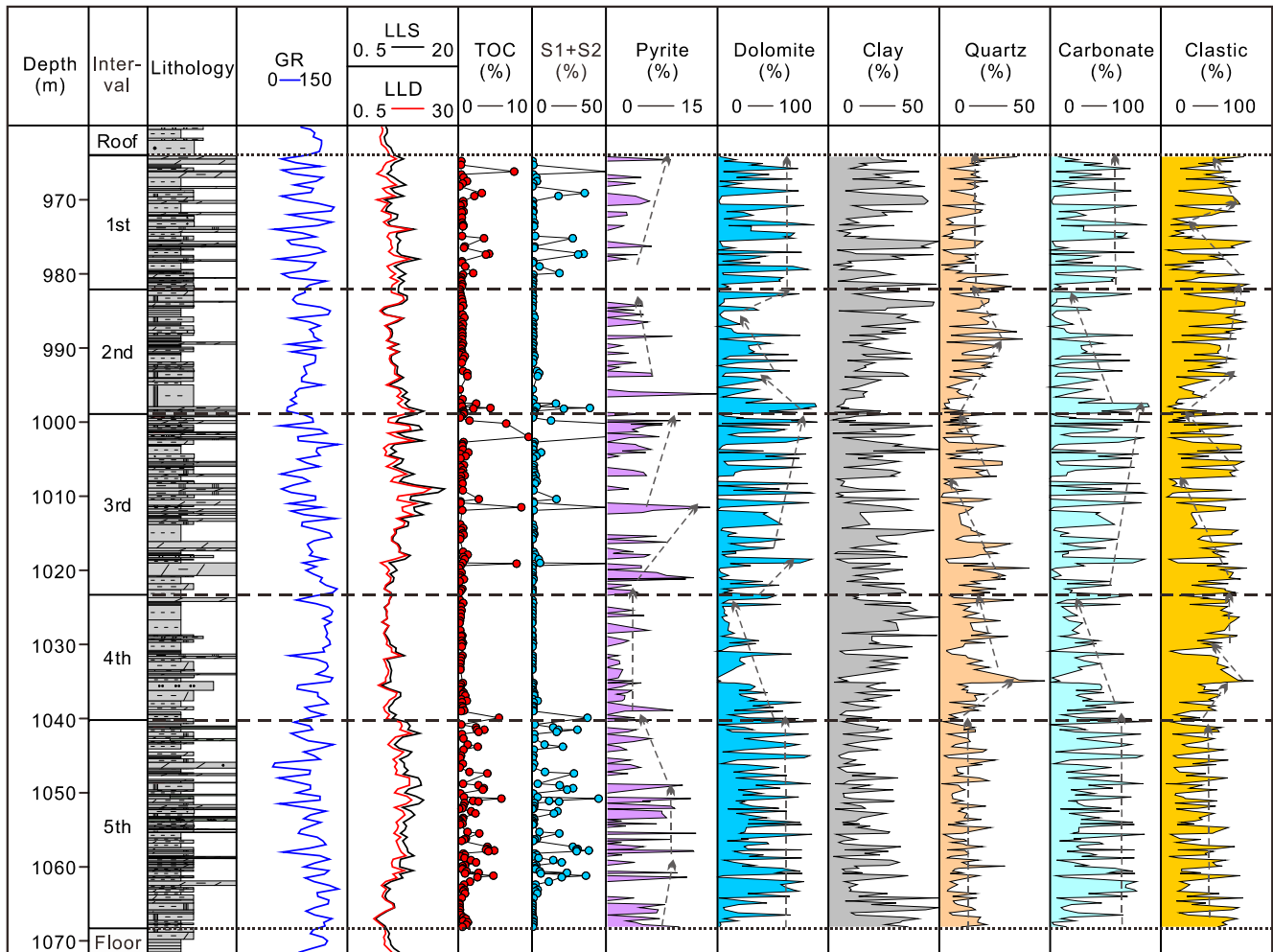


Figure 3. Lithological, geochemical, and mineralogical profiles of the LXF II Oil Bed in the Jiangnan Basin. Clastic = Quartz + Feldspar + Clay.

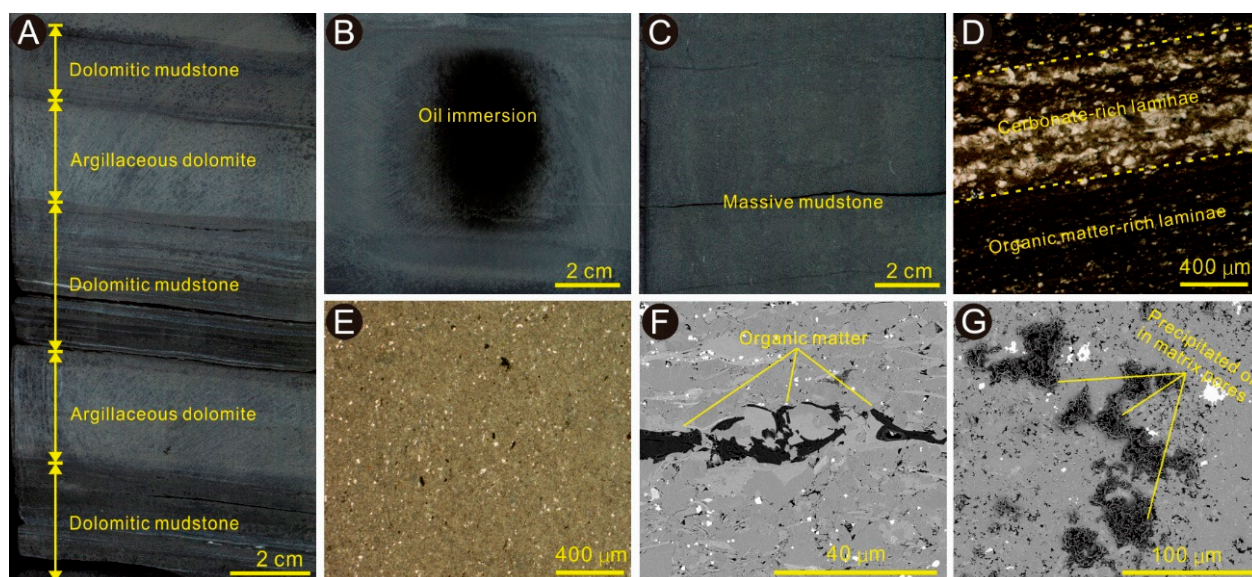


Figure 4. Core, thin section, and SEM images of the LXF II Oil Bed. (A) Dark gray laminated dolomitic mudstone and light gray massive argillaceous dolomite. (B) Oil immersion shown in argillaceous dolomite. (C) Gray massive mudstone. (D) Laminated mixed shale. Dark OM-rich laminae and light carbonate-rich laminae are observed. (E) Massive calcareous dolomitic shale. (F) Occurrence of solid OM in mixed shale. (G) Precipitated oil in matrix pores of calcareous dolomitic shale.

4.2. Reservoir Space

Shale pores not only provide space for hydrocarbon storage, but also form a flow-path network. Therefore, their size, type, and connectivity are essential for shale oil resource evaluation and development [33,34]. SEM images show that pores in the II Oil Bed are present in various types, having a wide range in morphology and size (Figure 5). Inorganic pores (intercrystalline pores, interparticle pores, and intraparticle pores related to the minerals) are dominant, with a few OM pores and micro-fractures (Figure 5). Dolomite grains are generally $<2\ \mu\text{m}$ and display perfect rhombic or sub-rhombic shapes (Figure 5A), and intercrystalline pores developed among them are the main reservoir space type (Figure 5B). Some intercrystalline pores are also developed in pyrite aggregates (Figure 5C), and these pores are interconnected. However, these aggregates are relatively isolated, and the pore size is small, so the oil in these pores may be difficult to extract. Interparticle pores mainly occur between clay platelets and detrital grains (Figure 5D). Intraparticle pores mainly include dissolution pores (Figure 5E) and halite skeleton pores (Figure 5F), and the former are usually related to the organic acids formed during hydrocarbon generation [35]. Only a few scattered OM pores were observed (Figure 5D). Since their formation is usually associated with hydrocarbon generation [1], the lack of OM pores may be the result of low maturity. Fractures can provide effective reservoir space, and can significantly improve fluid flow capacity. Therefore, they play an important role in shale oil exploration and development [36]. Many hydrocarbon-filled fractures can be observed, which serve as pathways for hydrocarbon migration (Figure 5G). In addition, clay shrinkage fractures were also observed, which were formed by the clay mineral transformation during diagenesis or low-grade metamorphism (Figure 5H), and some micro-fractures are now filled with halite (Figure 5I). Inevitably, however, fractures may also be caused by drying during sample preparation or dehydration after the core is collected to the surface [1].

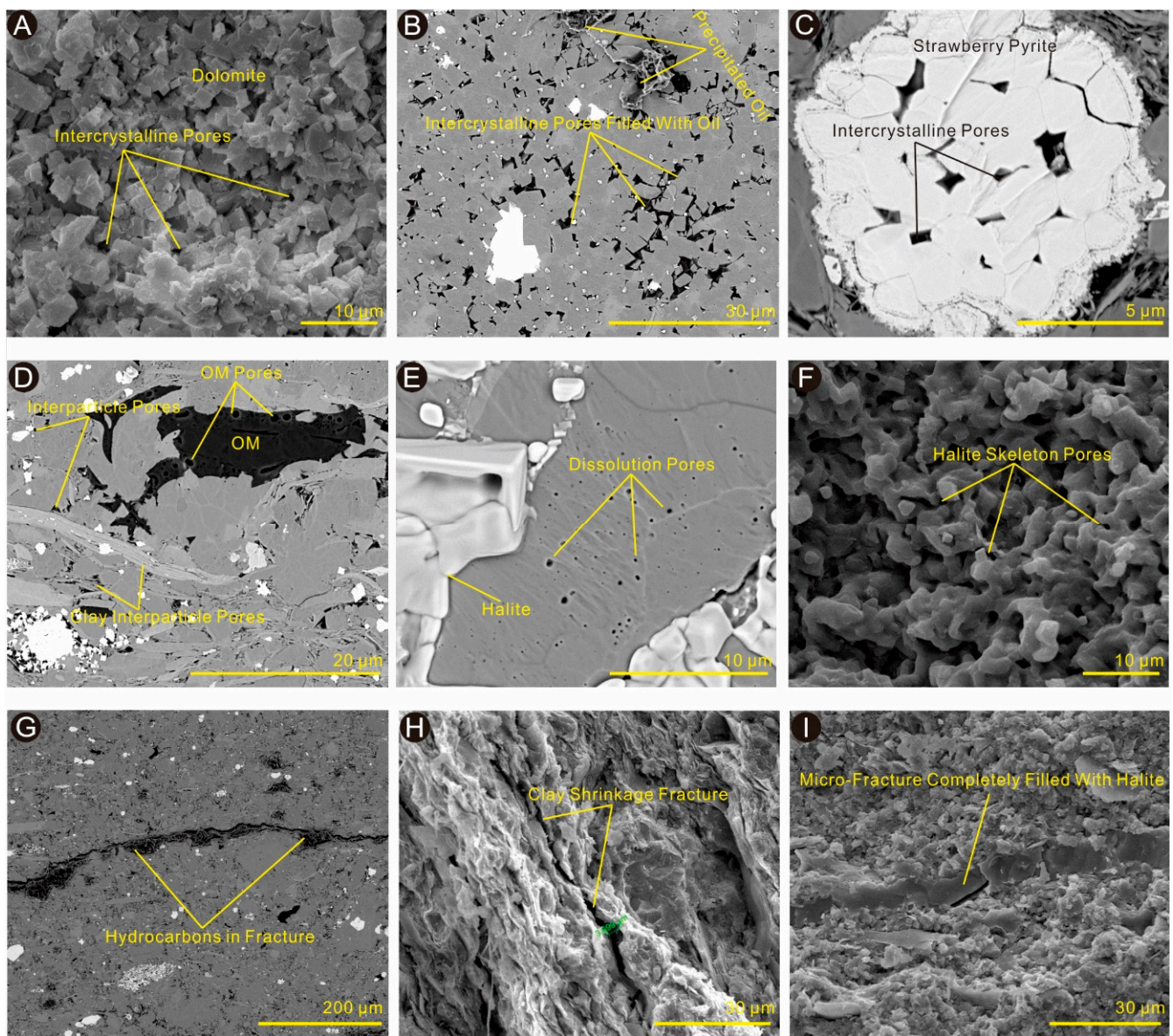


Figure 5. Representative pore types and fracture characteristics of the LXF II Oil Bed in the Jiangnan Basin. (A) Dolomite grains smaller than $2\ \mu\text{m}$ displaying perfect rhombic or sub-rhombic shape, among which, intercrystalline pores are developed. (B) Intercrystalline pores are usually filled with oil. (C) Intercrystalline pores within pyrite aggregate. (D) Interparticle pores between grains and clay platelets. Rare and scattered OM pores developed in OM. (E) Dissolution pores within feldspar. (F) Pores within halite skeleton. (G) Fractures filled with hydrocarbons. (H) Clay mineral shrinkage fracture. (I) Micro-fracture filled with halite.

The above pore types are developed to various degrees in different lithofacies. Due to the high carbonate content, CDS mainly develops carbonate mineral intercrystalline pores and dissolution pores, whereas MS develops relatively more interparticle pores. In addition, the mercury intrusion/extrusion curves show that the CDS have lower entry pressures and higher mercury removal efficiency than MS, indicating better pore connectivity (Figure 6A,B).

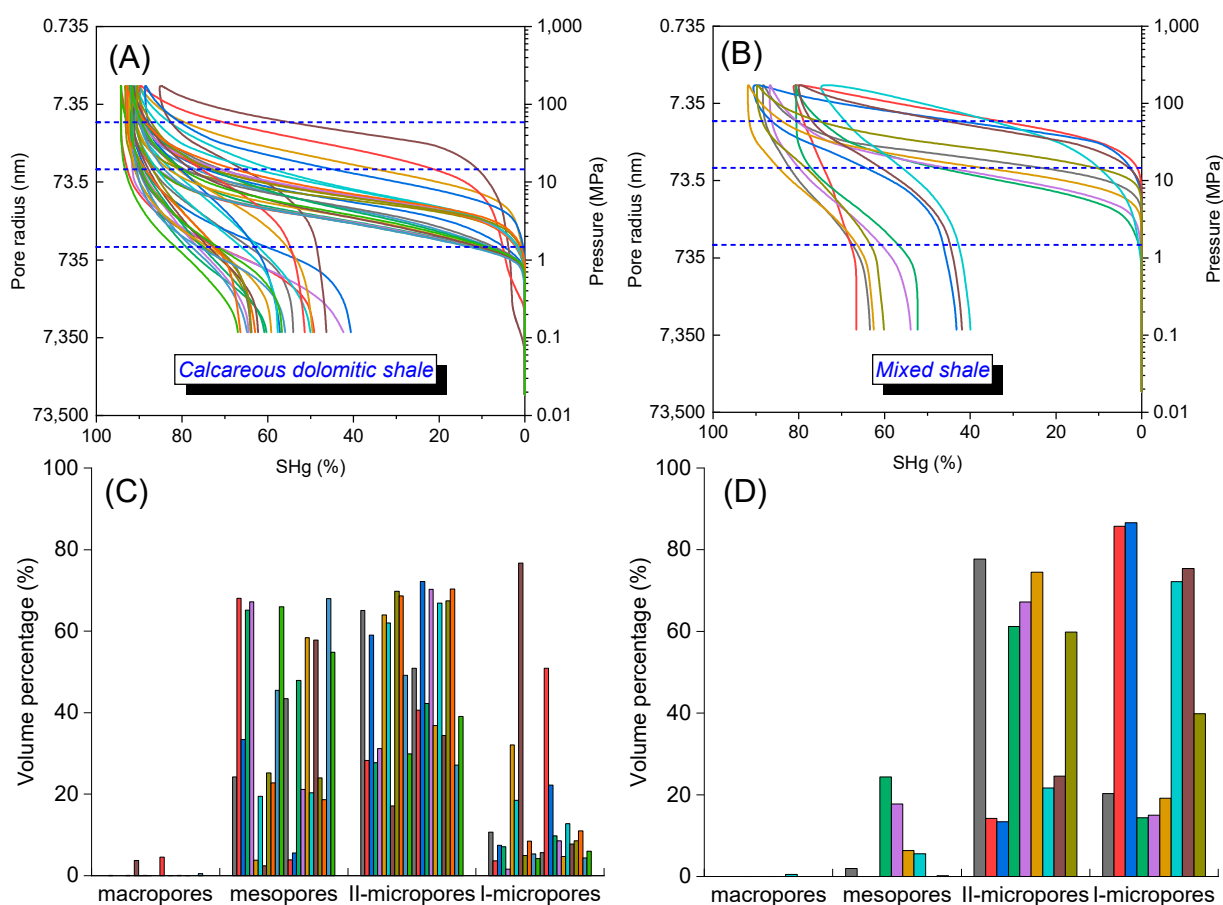


Figure 6. Mercury intrusion/extrusion curves of calcareous dolomitic shales (A) and mixed shales (B). Volume percentage of pores with different sizes in calcareous dolomitic shales (C) and mixed shales (D), macropores (>1000 nm), mesopores (100–1000 nm), II-micropores (25–100 nm), and I-micropores (<25 nm).

4.3. Hydrocarbon Generation Potential

OM abundance can reflect the hydrocarbon generation potential of source rocks [37]. It is usually evaluated by TOC and S1 + S2 [38], which range from 0.12–11.12% (avg. 1.09%) and 0.1–82.35 mg HC/g rock (avg. 5.42 mg HC/g rock), respectively (Figure 7). It is reported that, in the saline lacustrine environment, the source rocks with TOC > 0.6% are fair, and the high hydrocarbon conversion efficiency makes it possible to generate large amounts of hydrocarbons at the low-maturity stage [39]. The plot of TOC vs. S1 + S2 shows that most samples belong to a fair-to-very-good source rock, and the OM abundance of the 1st, 3rd, and 5th intervals are higher (Figure 7). OM type determines whether the source rock is oil- or gas-prone [37]. The HI values of the studied samples ranged from 12.25–924.39 mg HC/g TOC (avg. 249.29 mg HC/g TOC) ($HI = S2/TOC \times 100$) [38] (Figure 8A). The plot of HI vs. Tmax shows that the sample points are widely distributed within the region of Type II, with a certain amount of Type I and Type III (Figure 8A), whereas the type index (TI) indicates that they are mainly Type II₁ and Type II₂ (Figure 8B). The Ro and Tmax are usually applied to evaluate the OM maturity [37,40]. The studied samples display Tmax of 402–447 °C (avg. 426 °C), indicating that most of them are immature (Figures 8A and 9A), whereas Ro ranged from 0.48–1.07% (Figure 9B), supporting that the samples have low-to-peak oil window maturity [40]. Ro value varies greatly in different regions, reflecting the changes in thermal maturity or burial depth in different regions. Overall, the II Oil Bed has good hydrocarbon generation potential in terms of the quantity, quality, and maturity of OM.

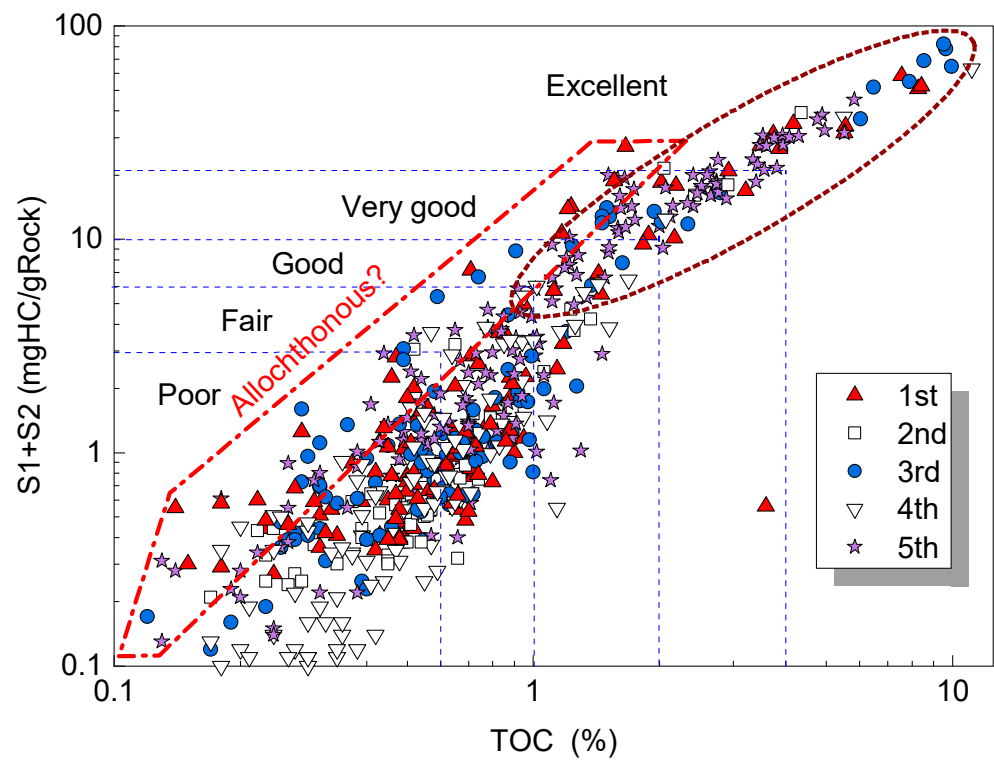


Figure 7. Cross-plot of S1 + S2 vs. TOC (after [37]).

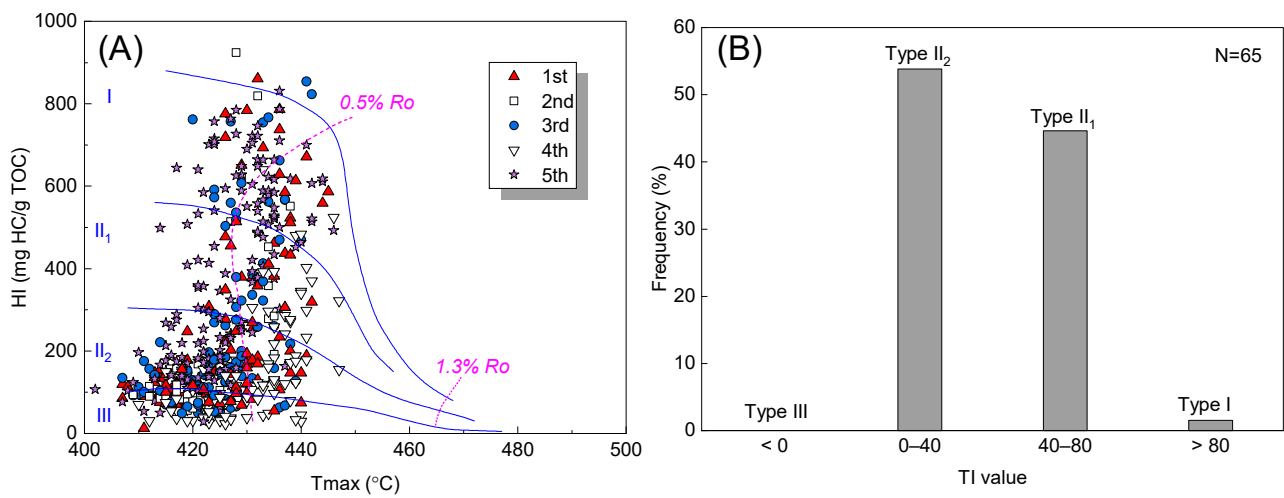


Figure 8. (A) Cross-plot of Tmax vs. HI (after [38]). (B) Frequency distribution of TI (type index), $TI = 100 \times (\text{sapropelinite, \%}) + 50 \times (\text{liptinite, \%}) - 75 \times (\text{virtrinite, \%}) - 100 \times (\text{inertinite, \%})$, and $TI > 80$, $80 > TI > 40$, $40 > TI > 0$, and $TI < 0$ indicate Type I, Type II₁, Type II₂, and Type III, respectively.

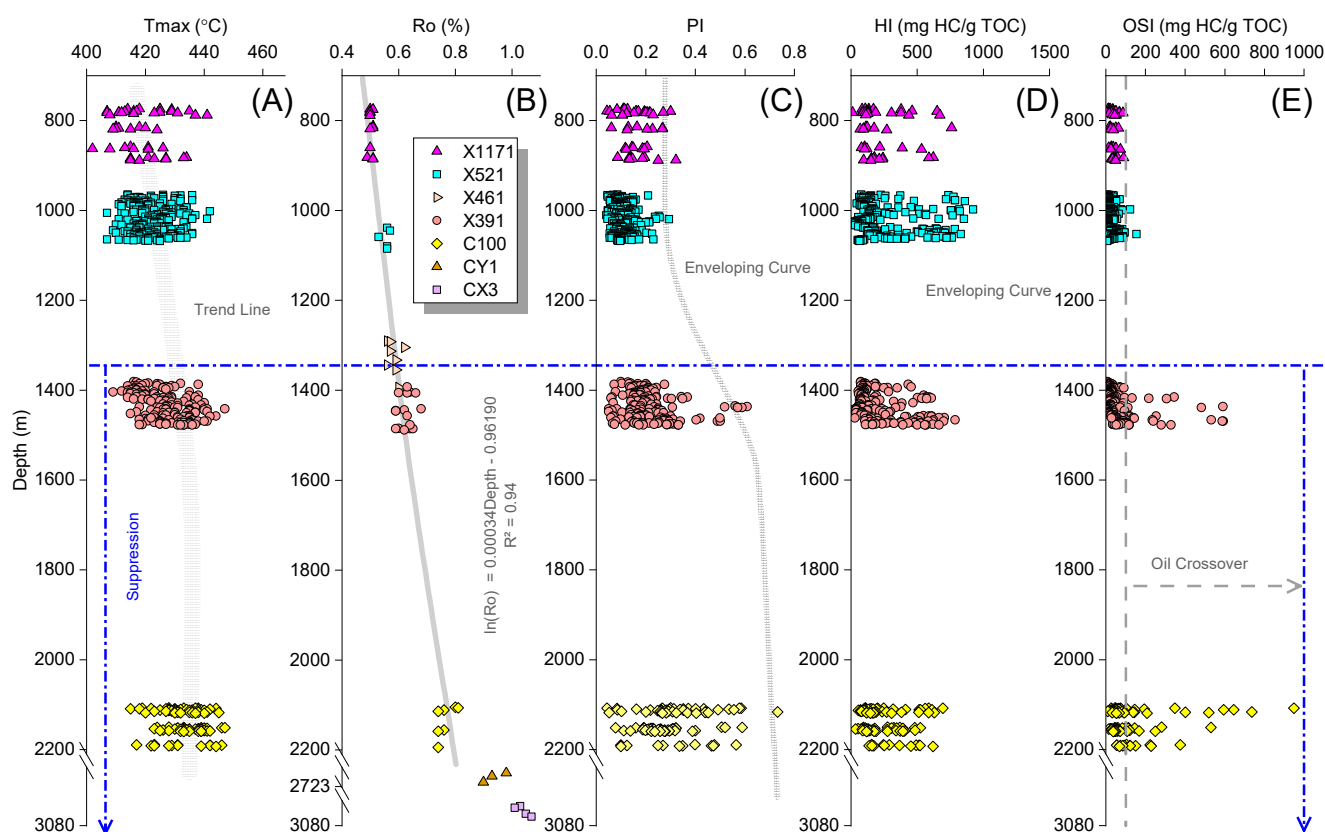


Figure 9. Geochemical profiles of wells with different buried depths. $PI = S1/(S1 + S2)$; $HI = S2/TOC \times 100$; $OSI = S1/TOC \times 100$. (A) Tmax vs. depth plot shows that Tmax are suppressed below 1350 m. (B) Ro vs. depth plot shows that Ro increases with burial depth. (C) PI vs. depth plot, $PI = S1/(S1 + S2)$. (D) HI vs. depth plot, $HI = S2/TOC \times 100$. (E) OSI vs. depth plot showing obvious oil crossover effect below 1350 m, $OSI = S1/TOC \times 100$.

5. Discussion

5.1. Brittleness and Reservoir Capacity

Rock brittleness is related to the mineral composition, and is an important index for shale oil potential evaluation [41]. In comparison with the mineralogical data of typical USA shales, the high carbonate and low clay content of the II Oil Bed is highlighted, which will facilitate the formation of natural fractures and hydraulic stimulation in the production process, as well as the development of dissolution pores [29,42], thus showing a good fracturing tendency (Figure 2C).

The Laplace–Washburn equation was adopted to calculate the pore radii corresponding to different pressures [43]. The pore size classification is based on the scheme proposed by Zhang et al. (2017), i.e., macropores (>1000 nm), mesopores (100–1000 nm), II-micropores (25–100 nm), and I-micropores (<25 nm) [27]. It is found that CDS mainly develops mesopores and a few macropores and II-micropores, whereas MS mainly develops II-micropores and a few mesopores and I-micropores (Figure 6C,D). According to the grading evaluation scheme established by Lu et al. (2018), CDS belongs to good Type2 reservoirs, whereas MS belongs to poor Type3 reservoirs [44]. This indicates that high carbonate content is conducive to the protection of pores and the formation of dissolution pores, thus forming more macropores and mesopores with good connectivity, whereas in clay minerals, it is easy to cause intergranular compaction and filling, with more developed micropores and poor connectivity [13,27]. Intercrystalline pores usually contain oil, fully demonstrating their effectiveness (Figure 5B). In addition, a recent study suggests that dissolution pores are important reservoir spaces for shale oil in the LXF [45], and dolomite greatly improves the porosity and permeability (the average porosity increased by dolomite dissolution

is 2.34%) [45]. Therefore, the reservoir capacity and connectivity of CDS are better than those of MS. Moreover, the pores developed in the II Oil Bed are large enough, and the pore-fracture system formed by its combination with widespread fractures facilitates oil flow and storage [33,46].

5.2. Applicability Evaluation of Bulk Geochemical Parameters

5.2.1. The “True” Organic Matter Abundance

Some studies have revealed the impact of intrasource migration on bulk geochemical analysis [47]. The plot of TOC vs. S1 + S2 shows that some samples from the 1st, 3rd, and 5th intervals have low TOC, but high S1 + S2, which may be related to allochthonous hydrocarbons [40]. The measured TOC in rocks includes the carbon in kerogen and hydrocarbons, and the latter may contain both generated hydrocarbons and migrated hydrocarbons. The kerogen organic carbon (TOC_k) was utilized to evaluate the hydrocarbon generation capacity of different lithofacies (TOC_k = TOC − 0.83 × extracts [48]). The results show that the average TOC_k values of CDS, CS, MS, and FS are 0.67, 2.91, 2.07, and 1.66, respectively (Figure 10). For the two main lithofacies, MS has a stronger hydrocarbon generation capacity than CDS. In addition, we propose a new evaluation parameter, “TOCs”, to characterize the state of OM in different lithofacies, which represents the proportion of organic carbon in soluble OM to TOC (TOCs = 0.83 × extracts/TOC × 100%). The average TOCs values of CDS, CS, MS, and FS are 40.78%, 6.72%, 17.92, and 1.49%, respectively (Figure 10), indicating that CDS contained more soluble OM, which is consistent with the observation of SEM images (Figure 4F,G). Therefore, it is speculated that the 2nd and 4th intervals, with more MS, have higher original OM content. On the contrary, the 1st, 3rd, and 5th intervals contain more allochthonous OM.

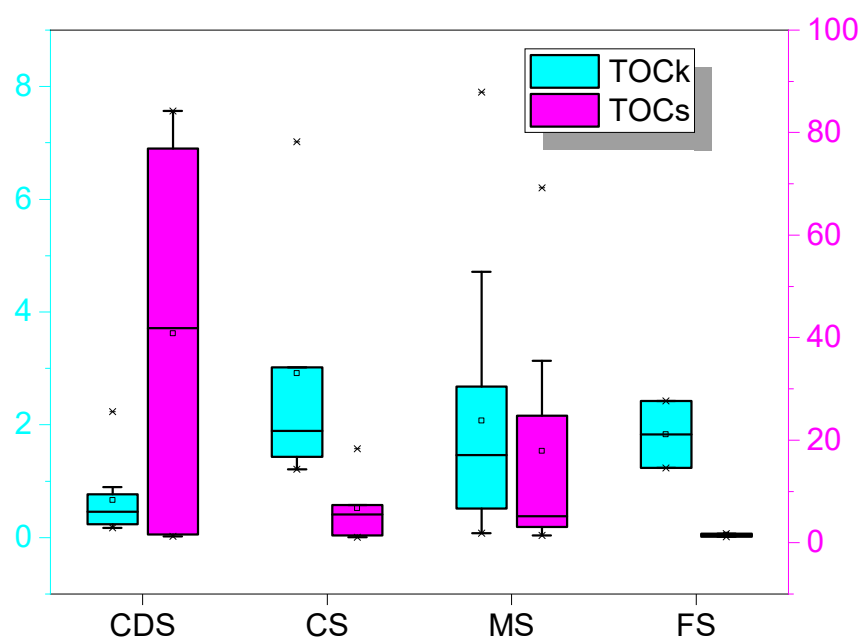


Figure 10. The kerogen organic carbon (TOC_k) and the proportion of organic carbon in soluble OM to TOC of different lithofacies show that MS has a stronger hydrocarbon generation capacity than CDS. TOC_k = TOC − 0.83 × extracts [48]. TOCs = 0.83 × extracts/TOC × 100%.

5.2.2. Paradox in Rock-Eval Pyrolysis and Visual Kerogen Compositions

The plot of S2 vs. TOC is useful to study the kerogen type [49,50], which shows a wide range of variation for both, but a strong linear correlation between them ($R^2 = 0.94$) (Figure 11A). The “true” HI (HI_L = 697 mg HC/g TOC) is close to that of the Type I kerogen, indicating the important contribution of aquatic organisms (Figure 11A). Samples with low HI (“true” HI < 200 mg HC/g TOC) are also observed (Figure 11B). These data deviate

from the previous trend, showing a strong OM type heterogeneity, especially when the TOC < 1% (Figure 11B).

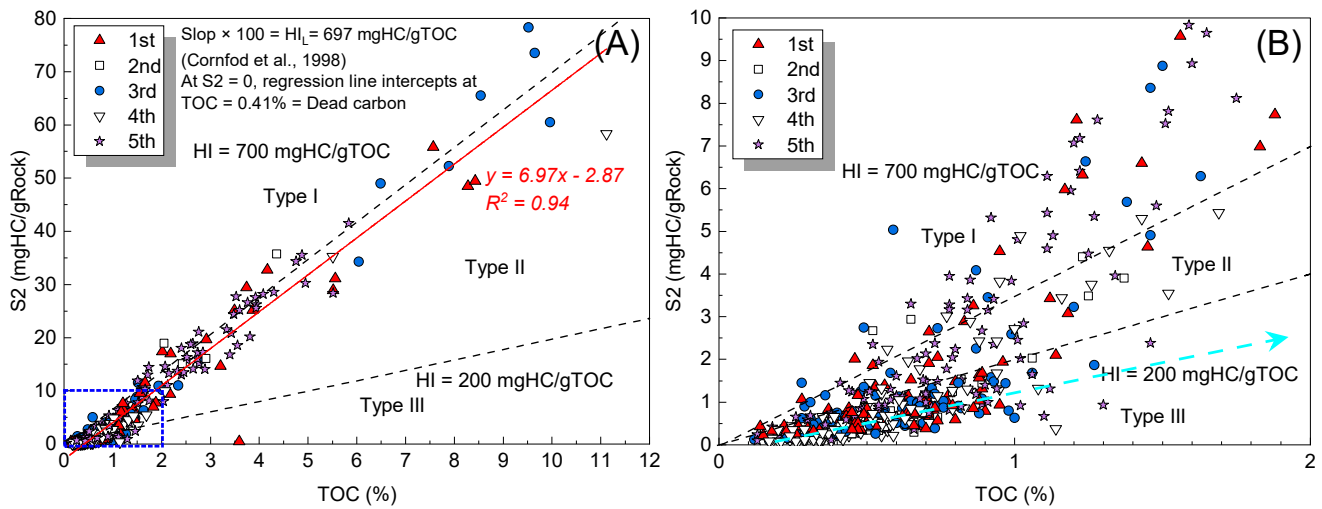


Figure 11. (A) S₂ vs. TOC plot showing the OM quantity and quality (after [49,50]). (B) An enlarged view of the blue box in (A).

Interestingly, samples with a low T_{max} also have a correspondingly low TOC, reflecting the existence of migrated hydrocarbons in many samples with TOC < 1% (Figure 12) [13]. If they are excluded, samples with TOC of 0–1% should have a more uniform HI and less Type III kerogen. In addition, Figure 9A shows that T_{max} values are suppressed below 1350 m, accompanied by a gradually increasing Ro (vitrinite reflectance) and PI (production index), and decreasing HI, as well as an obvious oil crossover effect in the suppression zone (Figure 9B–E). OM containing high hydrogen and bitumen content can cause T_{max} suppression [38,51]. It may be that these anomalously low T_{max} are plotted in the Type III region in Figure 8A, resulting in inconsistency with the maceral analyses. This explains why a certain amount of Type III kerogen was identified by pyrolysis parameters rather than by maceral analyses. In summary, the OM in the II Oil Bed is mainly Type II, and the above phenomena indicate that the hydrocarbons generated in adjacent source rocks have migrated to CDS.

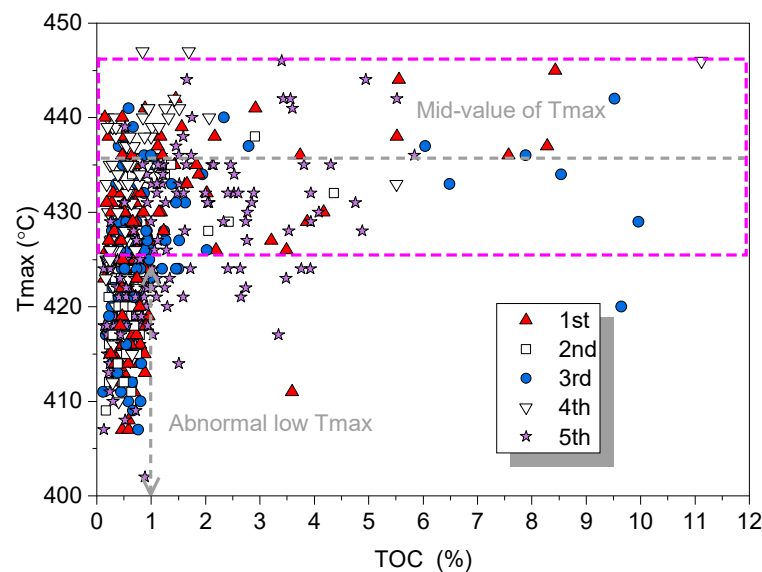


Figure 12. T_{max} vs. TOC plot showing the existence of migrated hydrocarbons in the samples with TOC < 1%.

5.3. Shale Oil Potential and Enrichment Model

Recent studies suggest that shales with Type II kerogen should be given priority in shale oil exploration [26,52]. Although Type I kerogen has the highest oil generation capacity, it also has the highest oil expulsion efficiency [53], which may result in a low residual oil content [26,52]. Moreover, Type I kerogen has low oxygen content, which is necessary for the formation of organic acids and secondary pores [54,55]. In addition, there is no consensus on the favorable maturity range for continental shale oil exploration, e.g., 0.5–1.5%Ro [56], 0.7–1.1%Ro [57], and 0.5–1.0%Ro [58]. This is mainly due to the different research objects and concerns of scholars. A recent study on lacustrine argillaceous dolomite shows that the content of retained hydrocarbons reached the maximum when Ro was between 0.6–1.3% [59]. Therefore, the II Oil Bed is currently in a favorable maturity range.

After the II Oil Bed deposition, the differential tectonic evolution leads to the variable burial depths in different parts of the study area (Figure 1C). The southern part experienced continuous subsidence, the maximum burial depth is >3000 m, and the source rock experienced a mature stage, with Ro generally between 0.7–1.0%. On the other hand, the burial depth of the northern part is generally <1000 m, and the minimum is only ~700 m, with lower thermal maturity (~0.5%Ro). The positive correlation between thermal evolution and burial depth indicates that it is controlled by burial depth, which is well-reflected in wells with different burial depths (Figure 9B). Finally, the deeper buried southern part entered the hydrocarbon generation threshold. According to the plot of Ro vs. depth, the corresponding buried depth of Ro = 0.6 is 1350 m (Figure 9B), with an obvious oil crossover effect and Tmax suppression (Figures 9A,E and 13).

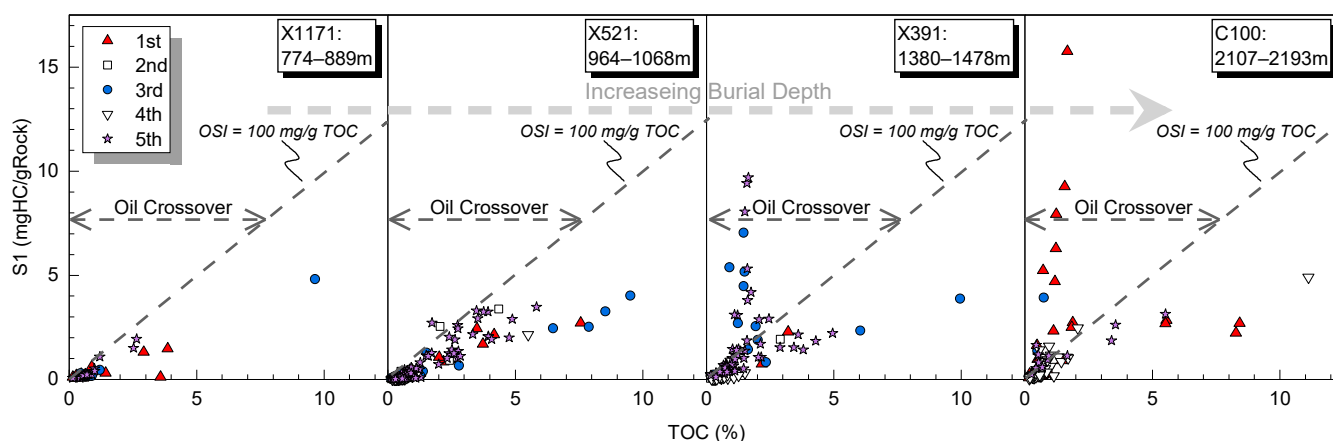


Figure 13. Control of thermal maturity on oil content is revealed by plotting the S1 vs. TOC of wells with different burial depths.

With the increasing burial depth, the II Oil Bed underwent diagenesis, e.g., compaction, clay mineral dehydration, dissolution, and hydrocarbon generation [6,60]. Especially after the middle diagenetic stage (Ro > 0.6), the carbonate-rich lithofacies (CDS) in the salt lake developed a high porosity zone dominated by secondary pores, which had obvious porosity enhancement and evolved into favorable lithofacies [45,60,61]. On the other hand, large quantities of hydrocarbons are generated in the OM-rich lithofacies (MS). Therefore, the middle-high evolution and high porosity zones are very consistent with the free oil window [60]. The latest research also shows that the pressure-induced “squeezing” effect will enhance hydrocarbon expulsion in ductile lithologies [62]. The concept of intrasource migration has also been well-known [14,63]. The oil generated by OM-rich lithofacies may be retained in their pores, or continue to be migrated to adjacent reservoirs with high porosity and permeability driven by abnormal pressure, forming a “self-generating and self-storing” petroleum system [14,18]. In this process, fractures are the main pathways for hydrocarbon migration (Figure 5G). Due to the high hydrocarbon generation potential of OM-rich lithofacies, with the conversion of high-density, solid kerogen to low-density,

liquid oil, the fluid volume expands, and the corresponding pore pressure increases [64], which facilitates the formation of fractures and the efficient escape of hydrocarbons. On the other hand, the carbonate-rich lithofacies are prone to develop secondary pores and natural fractures, which exist as pre-existing reservoir spaces, and are later filled with oil migrating from the generation site. However, in addition to lithofacies-scale intrasource migration, we suggest that the intrasource migrations are multi-scale, encompassing intervals. Indeed, small-scale intrasource migrations are often superimposed on larger ones, which results in the enrichment of hydrocarbons in the 1st, 3rd, and 5th intervals, and an oil crossover effect mainly occur in these intervals (Figure 13). In the sandwiched or interlayered configuration, source rocks are in close contact with reservoirs, which allows hydrocarbons to be directly charged nearby, and thus, have good oil-bearing properties. The intrasource migration of petroleum can alter the composition of fluids remaining in, and expelled from, the source rocks [65]. Thus, the most significant aspect for the petroleum industry is that this will produce the optimal targets or potential sweet spots in shale oil exploration and production. With the passage of geological time, hydrocarbons migrate and are expelled within the shale system, and stratigraphic fractionation makes them contain more aliphatic fractions, thereby improving the quality of oil [1,63]. The 1st, 3rd, and 5th intervals are a set of attractive targets for oil production based on the fact that the overall mineral composition indicates a high degree of brittleness, and is, therefore, conducive to hydraulic fracturing. Therefore, in this study, we have not only identified a set of promising targets, but also explained the differential enrichment of shale oil in the LXF, and presented a shale oil enrichment model based on this case study.

6. Summary and Conclusions

The LXF II Oil Bed in the Jiangnan Basin is rich in carbonate and poor in clay minerals, so it shows a good fracturing tendency. Pores in the II Oil Bed are present as various types, having a wide range in morphology and size, and the carbonate-rich lithofacies have a better reservoir capacity. In terms of the quantity and quality of OM, the II Oil Bed is a good source rock. Given its OM abundance generally ranges from fair to very good, with early-mature to mature Type II OM, the II Oil Bed is considered to have the characteristics required for oil generation.

The enrichment of shale oil in the II Oil Bed is the result of multiple factors matching. The strong heterogeneity of mineral composition also causes different lithofacies within the sequence to appear in the form of interbeds. Due to the differential post-depositional tectonic evolution, there are differences in the burial depth and thermal maturity between areas, which further controls the differential enrichment of shale oil in different areas. Pores and micro-fractures developed in shale not only provide space for hydrocarbon storage, but also form a flow-path network. Multi-scale intrasource migrations are key processes, and small-scale intrasource migrations are often superimposed on larger ones, which results in the differential shale oil enrichment in different intervals. Multiple factors in the shale oil enrichment model collectively account for the good productive potential of shale oil sweet-spot intervals (i.e., 1st, 3rd, and 5th intervals).

Through the comprehensive analysis of geological parameters, it is considered that the II Oil Bed has good shale oil exploration prospects. When evaluating planar shale oil sweet spots, emphasis should be placed on thickness, thermal maturity, or burial depth. Considering the hydrocarbon generation capacity and reservoir quality, the prospective depth for shale oil exploration in the study area is below 1350 m.

The advantages of this study are that it reveals the roles of thermal maturity and lithofacies in shale oil enrichment; it also proposes a new parameter to characterize the occurrence state of OM, and clarifies that multi-scale intrasource migration is a key process in shale oil enrichment. The disadvantages are that there is no quantitative evaluation of migrated hydrocarbons; however, the influence of oil content on the pore characterization of shale reservoirs has not been excluded.

Author Contributions: Q.L.: Conceptualization, Methodology, Writing—Original draft preparation; S.X.: Supervision, Writing—Review and Editing, Validation; L.Z.: Resources, Validation; F.C.: Data curation, Validation; S.W.: Validation; N.B.: Visualization. All authors have read and agreed to the published version of the manuscript.

Funding: This research was funded by the National Natural Science Foundation of China (42122017, 41821002), the Shandong Provincial Key Research and Development Program (2020ZLYS08), the Independent innovation research program of China University of Petroleum (East China) (21CX06001A), and the Open Fund of Key Laboratory of Tectonics and Petroleum Resources (China University of Geosciences), Ministry of Education, China (TPR-2021-17).

Institutional Review Board Statement: Not applicable.

Informed Consent Statement: Not applicable.

Data Availability Statement: The data presented in this study are available on request from the corresponding author.

Conflicts of Interest: We declare that we have no financial and personal relationships with other people or organizations that can inappropriately influence our work, and there is no professional or other personal interest of any nature or kind in any product, service, and/or company that could be construed as influencing the position presented in the manuscript.

Nomenclature

| | |
|------------------|---|
| OM | organic matter |
| TOC | total organic carbon, % |
| S1 | free hydrocarbons, mg HC/g Rock |
| S2 | kerogen cracking hydrocarbons, mg HC/g Rock |
| Tmax | the temperature at which S2 generation rate is maximum, °C |
| HI | hydrogen index, $HI = S2/TOC \times 100$, mg HC/g TOC |
| PI | production index, $PI = S1/(S1 + S2)$ |
| OSI | oil saturation index, $OSI = S1/TOC \times 100$, mg HC/g TOC |
| TOC _k | kerogen organic carbon, $TOC_k = TOC - 0.83 \times \text{extracts}$ |
| TOC _s | proportion of organic carbon in soluble OM to TOC, $TOC_s = 0.83 \times \text{extracts}/TOC \times 100\%$ |
| Ro | vitrinite reflectance, % |

References

- Jarvie, D.M. Shale resource systems for oil and gas: Part 2—Shale-oil resource systems. In *Shale Reservoirs—Giant Resources for the 21st Century*; Breyer, J.A., Ed.; AAPG Memoir: Humble, TX, USA, 2012; Volume 97, pp. 89–119.
- Gou, Q.; Xu, S.; Hao, F.; Zhang, B.; Shu, Z.; Yang, F.; Wang, Y.; Li, Q. Quantitative calculated shale gas contents with different lithofacies: A case study of Fuling gas shale, Sichuan Basin, China. *J. Nat. Gas Sci. Eng.* **2020**, *76*, 103222. [[CrossRef](#)]
- Xu, S.; Gou, Q.; Hao, F.; Zhang, B.; Shu, Z.; Zhang, Y. Multiscale faults and fractures characterization and their effects on shale gas accumulation in the Jiaoshiba area, Sichuan Basin, China. *J. Pet. Sci. Eng.* **2020**, *189*, 107026. [[CrossRef](#)]
- Vo Thanh, H.; Sugai, Y.; Sasaki, K. Application of artificial neural network for predicting the performance of CO₂ enhanced oil recovery and storage in residual oil zones. *Sci. Rep.* **2020**, *10*, 18204. [[CrossRef](#)]
- Thanh, H.V.; Sugai, Y.; Nguete, R.; Sasaki, K. Integrated workflow in 3D geological model construction for evaluation of CO₂ storage capacity of a fractured basement reservoir in Cuu Long Basin, Vietnam. *Int. J. Greenh. Gas Control* **2019**, *90*, 102826. [[CrossRef](#)]
- Liu, C.; Wang, Z.; Guo, Z.; Hong, W.; Dun, C.; Zhang, X.; Li, B.; Wu, L. Enrichment and distribution of shale oil in the Cretaceous Qingshankou formation, Songliao basin, northeast China. *Mar. Pet. Geol.* **2017**, *86*, 751–770. [[CrossRef](#)]
- Bohacs, K.M.; Carroll, A.R.; Neal, J.E.; Mankiewicz, P.J. Lake-basin type, source potential, and hydrocarbon character: An integrated sequence-stratigraphic-geochemical framework. In *Lake Basins Through Space and Time*; AAPG Studies in Geology; American Association of Petroleum: Tulsa, OK, USA, 2000; Volume 46, pp. 3–34.
- Hao, F.; Zhou, X.; Zhu, Y.; Yang, Y. Lacustrine source rock deposition in response to co-evolution of environments and organisms controlled by tectonic subsidence and climate, Bohai Bay Basin, China. *Org. Geochem.* **2011**, *42*, 323–339. [[CrossRef](#)]
- Hao, F.; Zhou, X.; Zhu, Y.; Zou, H.; Bao, X.; Kong, Q. Mechanisms of petroleum accumulation in the Bozhong sub-basin, Bohai Bay Basin, China. Part 1: Origin and occurrence of crude oils. *Mar. Pet. Geol.* **2009**, *26*, 1528–1542. [[CrossRef](#)]
- Vo Thanh, H.; Sugai, Y.; Sasaki, K. Impact of a new geological modelling method on the enhancement of the CO₂ storage assessment of E sequence of Nam Vang field, offshore Vietnam. *Energy Sources Part A Reco. Util. Environ. Eff.* **2020**, *42*, 1499–1512. [[CrossRef](#)]

11. Thanh, H.V.; Sugai, Y. Integrated modelling framework for enhancement history matching in fluvial channel sandstone reservoirs. *Upstream Oil Gas Technol.* **2021**, *6*, 100027. [[CrossRef](#)]
12. Lu, S.; Xue, H.; Wang, M.; Xiao, D.; Huang, W.; Li, J.; Xie, L.; Tian, S.; Wang, S.; Li, J. Several key issues and research trends in evaluation of shale oil. *Acta Pet. Sin.* **2016**, *37*, 1309–1322.
13. Liu, B.; Wang, H.; Fu, X.; Bai, Y.; Bai, L.; Jia, M.; He, B. Lithofacies and depositional setting of a highly prospective lacustrine shale oil succession from the Upper Cretaceous Qingshankou Formation in the Gulong sag, northern Songliao Basin, northeast China. *AAPG Bull.* **2019**, *103*, 405–432. [[CrossRef](#)]
14. Han, Y.; Horsfield, B.; Curry, D.J. Control of facies, maturation and primary migration on biomarkers in the Barnett Shale sequence in the Marathon 1 Mesquite well, Texas. *Mar. Pet. Geol.* **2017**, *85*, 106–116. [[CrossRef](#)]
15. Xu, S.; Gou, Q.; Hao, F.; Zhang, B.; Shu, Z.; Lu, Y.; Wang, Y. Shale pore structure characteristics of the high and low productivity wells, Jiaoshiba Shale Gas Field, Sichuan Basin, China: Dominated by lithofacies or preservation condition? *Mar. Pet. Geol.* **2020**, *114*, 104211. [[CrossRef](#)]
16. Carroll, A.R.; Bohacs, K.M. Stratigraphic classification of ancient lakes: Balancing tectonic and climatic controls. *Geology* **1999**, *27*, 99–102. [[CrossRef](#)]
17. Bai, C.; Yu, B.; Han, S.; Shen, Z. Characterization of lithofacies in shale oil reservoirs of a lacustrine basin in eastern China: Implications for oil accumulation. *J. Pet. Sci. Eng.* **2020**, *195*, 107907. [[CrossRef](#)]
18. Hu, S.; Li, S.; Xia, L.; Lv, Q.; Cao, J. On the internal oil migration in shale systems and implications for shale oil accumulation: A combined petrological and geochemical investigation in the Eocene Nanxiang Basin, China. *J. Pet. Sci. Eng.* **2020**, *184*, 106493. [[CrossRef](#)]
19. Hackley, P.C.; Fishman, N.; Wu, T.; Baugher, G. Organic petrology and geochemistry of mudrocks from the lacustrine Lucaogou Formation, Santanghu Basin, northwest China: Application to lake basin evolution. *Int. J. Coal Geol.* **2016**, *168*, 20–34. [[CrossRef](#)]
20. Yang, Z.; Zou, C.; Hou, L.; Wu, S.; Lin, S.; Luo, X.; Zhang, L.; Zhao, Z.; Cui, J.; Pan, S. Division of fine-grained rocks and selection of “sweet sections” in the oldest continental shale in China: Taking the coexisting combination of tight and shale oil in the Permian Junggar Basin. *Mar. Pet. Geol.* **2019**, *109*, 339–348. [[CrossRef](#)]
21. Huang, C.; Hinnov, L.A. Evolution of an Eocene-Oligocene saline lake depositional system and its controlling factors, Jiangnan Basin, China. *J. Earth Sci.* **2014**, *25*, 959–976. [[CrossRef](#)]
22. Li, Q.; Xu, S.; Hao, F.; Shu, Z.; Chen, F.; Lu, Y.; Wu, S.; Zhang, L. Geochemical characteristics and organic matter accumulation of argillaceous dolomite in a saline lacustrine basin: A case study from the paleogene xingouzui formation, Jiangnan Basin, China. *Mar. Pet. Geol.* **2021**, *128*, 105041. [[CrossRef](#)]
23. Tian, Z.; Han, P.; Xu, K. The Mesozoic–Cenozoic East China rift system. *Tectonophysics* **1992**, *208*, 341–363. [[CrossRef](#)]
24. Li, J.; Zhang, Y.; Dong, S.; Johnston, S.T. Cretaceous tectonic evolution of South China: A preliminary synthesis. *Earth Sci. Rev.* **2014**, *134*, 98–136. [[CrossRef](#)]
25. Molnar, P.; Tapponnier, P. Cenozoic tectonics of Asia: Effects of a continental collision. *Science* **1975**, *189*, 419–426. [[CrossRef](#)] [[PubMed](#)]
26. Li, W.; Lu, S.; Xue, H.; Zhang, P.; Hu, Y. Oil content in argillaceous dolomite from the Jiangnan Basin, China: Application of new grading evaluation criteria to study shale oil potential. *Fuel* **2015**, *143*, 424–429. [[CrossRef](#)]
27. Zhang, P.; Lu, S.; Li, J.; Xue, H.; Li, W.; Zhang, P. Characterization of shale pore system: A case study of Paleogene Xin’gouzui Formation in the Jiangnan basin, China. *Mar. Pet. Geol.* **2017**, *79*, 321–334. [[CrossRef](#)]
28. Mba, K.; Prasad, M. Mineralogy and its contribution to anisotropy and kerogen stiffness variations with maturity in the Bakken Shales. In *SEG Technical Program Expanded Abstracts 2010*; Society of Exploration Geophysicists: Houston, TX, USA, 2010; pp. 2612–2616.
29. Chalmers, G.R.; Bustin, R.M.; Power, I.M. Characterization of gas shale pore systems by porosimetry, pycnometry, surface area, and field emission scanning electron microscopy/transmission electron microscopy image analyses: Examples from the Barnett, Woodford, Haynesville, Marcellus, and Doig units. *Characterization of Gas Shale Pore Systems. AAPG Bull.* **2012**, *96*, 1099–1119.
30. Demaison, G.J.; Moore, G.T. Anoxic environments and oil source bed genesis. *AAPG Bull.* **1980**, *64*, 1179–1209. [[CrossRef](#)]
31. Zolitschka, B.; Francus, P.; Ojala, A.E.; Schimmelmann, A. Varves in lake sediments—A review. *Quat. Sci. Rev.* **2015**, *117*, 1–41. [[CrossRef](#)]
32. Zhao, X.; Pu, X.; Zhou, L.; Jin, F.; Shi, Z.; Han, W.; Jiang, W.; Zhang, W. Typical geological characteristics and exploration practices of lacustrine shale oil: A case study of the Kong-2 member strata of the Cangdong Sag in the Bohai Bay Basin. *Mar. Pet. Geol.* **2020**, *113*, 103999.
33. Ross, D.J.; Bustin, R.M. The importance of shale composition and pore structure upon gas storage potential of shale gas reservoirs. *Mar. Pet. Geol.* **2009**, *26*, 916–927. [[CrossRef](#)]
34. Tian, H.; Pan, L.; Xiao, X.; Wilkins, R.W.; Meng, Z.; Huang, B. A preliminary study on the pore characterization of Lower Silurian black shales in the Chuandong Thrust Fold Belt, southwestern China using low pressure N₂ adsorption and FE-SEM methods. *Mar. Pet. Geol.* **2013**, *48*, 8–19. [[CrossRef](#)]
35. Barth, T.; Borgund, A.E.; Hopland, A.L. Generation of organic compounds by hydrous pyrolysis of Kimmeridge oil shale—Bulk results and activation energy calculations. *Org. Geochem.* **1989**, *14*, 69–76. [[CrossRef](#)]
36. Jiu, K.; Ding, W.; Huang, W.; Zhang, Y.; Zhao, S.; Hu, L. Fractures of lacustrine shale reservoirs, the Zhanhua Depression in the Bohai Bay Basin, eastern China. *Mar. Pet. Geol.* **2013**, *48*, 113–123. [[CrossRef](#)]

37. Tissot, B.P.; Welte, D.H. *Petroleum Formation and Occurrence*; Springer: New York, NY, USA, 1984.
38. Peters, K.E. Guidelines for evaluating petroleum source rock using programmed pyrolysis. *AAPG Bull.* **1986**, *70*, 318–329.
39. Zhang, Z.; Yang, F.; Li, D.; Fang, Z. The organic geochemistry research progress in Cenozoic salified lake in China. *Adv. Earth Sci.* **2000**, *15*, 65–70.
40. Hunt, J.M. *Petroleum Geochemistry and Geology*, 2nd ed.; W.H. Freeman and Company: New York, NY, USA, 1996.
41. Enderlin, M.B.; Alsleben, H.; Beyer, J.A. *Predicting Fracability in Shale Reservoirs*; AAPG: Tulsa, OK, USA, 2011.
42. Loucks, R.G.; Reed, R.M.; Ruppel, S.C.; Hammes, U. Spectrum of pore types and networks in mudrocks and a descriptive classification for matrix-related mudrock pores. *AAPG Bull.* **2012**, *96*, 1071–1098. [[CrossRef](#)]
43. Washburn, E.W. The dynamics of capillary flow. *Phys. Rev.* **1921**, *17*, 273. [[CrossRef](#)]
44. Lu, S.; Li, J.; Zhang, P.; Xue, H.; Wang, G.; Zhang, J.; Liu, H.; Li, Z. Classification of microscopic pore-throats and the grading evaluation on shale oil reservoirs. *Pet. Explor. Dev.* **2018**, *45*, 452–460. [[CrossRef](#)]
45. Li, W.; Kuang, Y.; Lu, S.; Cheng, Z.; Xue, H.; Shi, L. Porosity Enhancement Potential through Dolomite Mineral Dissolution in the Shale Reservoir: A Case Study of an Argillaceous Dolomite Reservoir in the Jiangnan Basin. *Energy Fuels* **2019**, *33*, 4857–4864. [[CrossRef](#)]
46. Hou, Y.; Wang, F.; He, S.; Dong, T.; Wu, S. Properties and shale oil potential of saline lacustrine shales in the Qianjiang Depression, Jiangnan Basin, China. *Mar. Pet. Geol.* **2017**, *86*, 1173–1190. [[CrossRef](#)]
47. Li, M.; Chen, Z.; Cao, T.; Ma, X.; Liu, X.; Li, Z.; Jiang, Q.; Wu, S. Expelled oils and their impacts on Rock-Eval data interpretation, Eocene Qianjiang Formation in Jiangnan Basin, China. *Int. J. Coal Geol.* **2018**, *191*, 37–48. [[CrossRef](#)]
48. Gao, G.; Yang, S.; Ren, J.; Zhang, W.; Xiang, B. Geochemistry and depositional conditions of the carbonate-bearing lacustrine source rocks: A case study from the Early Permian Fengcheng Formation of Well FN7 in the northwestern Junggar Basin. *J. Pet. Sci. Eng.* **2018**, *162*, 407–418. [[CrossRef](#)]
49. Langford, F.; Blanc-Valleron, M.-M. Interpreting Rock-Eval pyrolysis data using graphs of pyrolyzable hydrocarbons vs. total organic carbon. *AAPG Bull.* **1990**, *74*, 799–804.
50. Cornford, C.; Gardner, P.; Burgess, C. Geochemical truths in large data sets. I: Geochemical screening data. *Org. Geochem.* **1998**, *29*, 519–530. [[CrossRef](#)]
51. Clementz, D.M. Effect of oil and bitumen saturation on source-rock pyrolysis. *AAPG Bull.* **1979**, *63*, 2227–2232.
52. Hu, T.; Pang, X.; Jiang, S.; Wang, Q.; Zheng, X.; Ding, X.; Zhao, Y.; Zhu, C.; Li, H. Oil content evaluation of lacustrine organic-rich shale with strong heterogeneity: A case study of the Middle Permian Lucaogou Formation in Jimusaer Sag, Junggar Basin, NW China. *Fuel* **2018**, *221*, 196–205. [[CrossRef](#)]
53. Stainforth, J.G. Practical kinetic modeling of petroleum generation and expulsion. *Mar. Pet. Geol.* **2009**, *26*, 552–572. [[CrossRef](#)]
54. Surdam, R.C.; Crossey, L.J.; Hagen, E.S.; Heasler, H.P. Organic-inorganic interactions and sandstone diagenesis. *AAPG Bull.* **1989**, *73*, 1–23.
55. Seewald, J.S. Organic-inorganic interactions in petroleum-producing sedimentary basins. *Nature* **2003**, *426*, 327–333. [[CrossRef](#)]
56. Zhang, J.; Lin, L.; Li, Y. Classification and evaluation of shale oil. *Earth Sci. Front.* **2012**, *19*, 322–331.
57. Lu, S.; Huang, W.; Chen, F.; Li, J.; Wang, M.; Xue, H.; Wang, W.; Cai, X. Classification and evaluation criteria of shale oil and gas resources: Discussion and application. *Pet. Explor. Dev.* **2012**, *39*, 268–276. [[CrossRef](#)]
58. Zhao, W.; Hu, S.; Hou, L. Connotation and strategic role of in-situ conversion processing of shale oil underground in the onshore China. *Pet. Explor. Dev.* **2018**, *45*, 563–572. [[CrossRef](#)]
59. Li, Z.; Zheng, L.; Jiang, Q.; Ma, Z.; Tao, G.; Xu, E.; Qian, M.; Liu, P.; Cao, T. Simulation of hydrocarbon generation and expulsion for lacustrine organic-rich argillaceous dolomite and its implications for shale oil exploration. *Earth Sci.* **2018**, *43*, 566–576.
60. Zhang, S.; Liu, H.; Liu, Y.; Wang, Y.; Wang, M.; Bao, Y.; Hu, Q.; Li, Z.; Zhang, S.; Yao, S. Main controls and geological sweet spot types in Paleogene shale oil rich areas of the Jiyang Depression, Bohai Bay basin, China. *Mar. Pet. Geol.* **2020**, *111*, 576–587. [[CrossRef](#)]
61. Zhang, L.; Chen, Z.; Li, Z.; Zhang, S.; Li, J.; Liu, Q.; Zhu, R.; Zhang, J.; Bao, Y. Structural features and genesis of microscopic pores in lacustrine shale in an oil window: A case study of the Dongying depression. *AAPG Bull.* **2019**, *103*, 1889–1924. [[CrossRef](#)]
62. Stockhausen, M.; Galimberti, R.; Elias, R.; Di Paolo, L.; Schwark, L. Expulsinator assessment of oil/gas generation and expulsion characteristics of different source rocks. *Mar. Pet. Geol.* **2021**, *129*, 105057. [[CrossRef](#)]
63. Zou, C.; Pan, S.; Horsfield, B.; Yang, Z.; Hao, S.; Liu, E.; Zhang, L. Oil retention and intrasource migration in the organic-rich lacustrine Chang 7 shale of the Upper Triassic Yanchang Formation, Ordos Basin, central China. *AAPG Bull.* **2019**, *103*, 2627–2663. [[CrossRef](#)]
64. Fan, Z.; Jin, Z.-H.; Johnson, S. Subcritical propagation of an oil-filled penny-shaped crack during kerogen-oil conversion. *Geophys. J. Int.* **2010**, *182*, 1141–1147. [[CrossRef](#)]
65. Leythaeuser, D.; Schaefer, R.; Radke, M. Geochemical effects of primary migration of petroleum in Kimmeridge source rocks from Brae field area, North Sea. I: Gross composition of C₁₅₊-soluble organic matter and molecular composition of C₁₅₊-saturated hydrocarbons. *Geochim. Cosmochim. Acta* **1988**, *52*, 701–713. [[CrossRef](#)]